RSI Technical Note 005

Converting shear-probe, thermistor and micro-conductivity signals into physical units

Rolf Lueck

2016-12-21

Rockland Scientific International Inc.
520 Dupplin Rd
Victoria, BC, CANADA, V8Z 1C1
www.rocklandscientific.com

Contents

List of Figures

History

- 2010-02-06 RGL, Previous Version, MS-Word format
- 2016-12-21 RGL, Latex Version, Expanded thermistor and micro-conductivity sensor sections.

1 Introduction

This document describes how to convert data collected with a Rockland Scientific International Inc. (RSI) instrument into physical units for the shear-probe, FP07 thermistor and SBE7 micro-conductivity signals, and for their gradients in the direction of profiling.

The methods described here are implemented by the function `odas_p2mat.m` of the ODAS Matlab Library, version 4.2 and higher, which is supplied to all owners of RSI instruments. The function `odas_p2mat.m` converts raw data files into Matlab mat-files to support further data processing.

2 Shear probe fundamentals

The shear probe, also frequently called the ”air-foil” probe, was conceived by H. S. Ribner and T. Siddon at the University of Toronto [1]. It was adapted for use in water by T. Osborn who first used it in the ocean in 1972 [2]. Since then, it has become the standard sensor for measuring oceanic turbulence at dissipation scales.

The shear probe consists of a piezo-ceramic bender that is mounted into the end of a stainless steel sting with about one half of the length of the bender protruding outward (Figure 1). The bender produces a charge in response to a bending force. In the frequency range of oceanic turbulence ($\sim$1 – 100 Hz), the impedance of the ceramic is extremely high (greater than $\sim$1 GΩ). RSI uses a proprietary Teflon isolation to block moisture from reaching the bender, so that the impedance of the probe remains extremely high ($\sim$50 GΩ), indefinitely. A soft and pliable silicone-rubber covers the assembly in an axial-symmetric form. The shape of the probe tip is similar to a bullet.

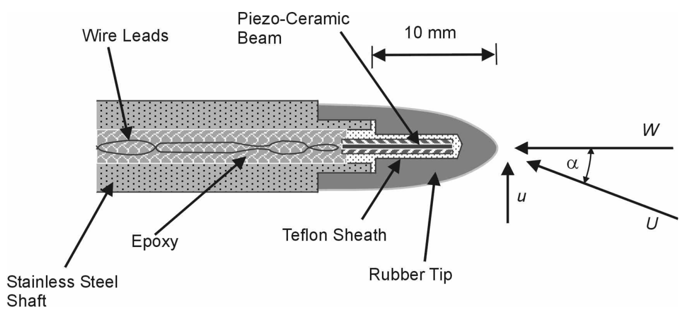

Figure 1: Sketch of a shear probe and the relevant velocity vectors.

The bender is 1.5 mm wide and 0.5 mm thick. It bends far more easily in its thin direction than in the other directions. (This is somewhat like a diving board at a pool which bends easily in one direction only.) Thus, the shear probe responds only to the component of velocity perpendicular to the broad side of the bender (the u component indicated in Figure 1). A flat surface is milled into the side of the shear probe body and this flat is parallel to the broad side of the bender. The flat is used to orient the probes when they are being mounted into their holders on the front of an instrument. To measure two orthogonal components of velocity fluctuations (u and v), two probes must be installed side-by-side with one probe rotated by 90° around its longitudinal axis so that the pair sense orthogonal components of velocity fluctuations.

The shear probe responds linearly to cross-stream velocity fluctuations when the angle of attack is small, $|\alpha| \lesssim 20°$. A velocity component orthogonal to the axis of the probe produces a pressure difference across the tip of the probe and this bends the beam very slightly. A detailed discussion can be found in [3]. Bending the beam produces a charge given by

$$
\begin{aligned}
Q_P &= \sqrt{2}\hat{S}U^2 \sin(2\alpha) \\
&= 2\sqrt{2}\hat{S}(U\cos\alpha)(U\sin\alpha) \\
&= 2\sqrt{2}\hat{S}Wu
\end{aligned}
\tag{1}
$$

where U is the total velocity vector, W is the velocity along the axis of the probe, u is the velocity orthogonal to the axis of the probe (and normal to the broad face of the ceramic beam), and $\hat{S}$ is the sensitivity of the probe (Figure 1). The factor of $2\sqrt{2}$ is an artifact of the method of calibration. Typical sensitivities are in the range of $\hat{S} = 0.05 - 0.10 \times 10^{-9}\,\mathrm{C\,m^2\,s^{-2}}$. This value is slightly temperature dependent and increases with increasing temperature. The symbol C stands for coulombs – a unit of charge.

There are two ways to capture the signal produced by a shear probe – a charge-transfer amplifier and a high-impedance voltage amplifier. Calibrations can be made with either type of amplifier with the calibration facility at RSI. All instruments produced by RSI use a charge-transfer amplifier. With a charge transfer amplifier, the charge produced by the shear probe is continuously removed and transferred to a capacitor of known value and exceptional temperature and aging stability ($1 \times 10^{-4}\,{}^{\circ}\mathrm{C}^{-1}$). The output voltage of the charge-transfer amplifier is the probe charge divided by the capacitance, namely

$$E_I = \frac{Q_P}{C_I} = \frac{2\sqrt{2}\hat{S}Wu}{C_I} \tag{2}$$

where the subscript I refers to the capacitor in the charge-transfer amplifier in an instrument. The charge-transfer amplifier actively holds the voltage across the ceramic beam in a shear probe at zero. Thus, the lead capacitance of the connection between the shear probe and the amplifier does not effect the output given by (2).

The shear probe is calibrated by rotating it at 1 Hz in a water jet of known flow and by varying the angle of attack of the jet with respect to the axis of the probe [3]. The signal produced by the probe is sinusoidal and has a frequency of 1 Hz. We measure the rms voltage of the output of the charge-transfer amplifier in the calibrator. The capacitor used in the charge-transfer amplifier in the calibrator has a value of $C_C = 1.50\,\mathrm{nF} \pm 1\,\%$. This rms voltage divided by the speed squared is then regressed against $\sin(2\alpha)$ to derive the sensitivity of the probes. The sensitivity is the slope of the best fit of

$$\frac{E_C^{rms}}{U^2} \text{ versus } \sin(2\alpha) \tag{3}$$

Where E_C^{rms} is the root-mean-square (rms) voltage produced by the shear probe. Using the rms voltage rather than the peak voltage accounts for the factor of $\sqrt{2}$ in equation (1). Thus, the peak voltage produced by the probe in the calibrator is

$$\begin{aligned} E_C &= \frac{Q_P}{C_C} \\ &= \frac{\sqrt{2}\hat{S}U^2}{C_C}\sin(2\alpha) \\ &= \frac{2\sqrt{2}\hat{S}Wu}{C_C} \\ &= 2\sqrt{2}SWu \end{aligned} \tag{4}$$

where the subscripts C refer to the calibrator and we have defined

$$S = \frac{\hat{S}}{C_C} \; . \tag{5}$$

The sensitivity value S is provided with the calibration certificate of each probe and typically falls in the range of 0.05–0.10 $\mathrm{V\,m^{-2}\,s^2}$.

The capacitor in the charge-transfer amplifier in instruments manufactured by RSI is usually $C_I = 1.50\,\mathrm{nF}$. The temperature coefficient of this capacitor is less than $1 \times 10^{-4}\,^\circ\mathrm{C}^{-1}$. It is intentionally chosen to equal the capacitor used in the calibrator. The voltage produced by the charge-transfer amplifier in an instrument is

$$E_I = \frac{2\sqrt{2}\hat{S}Wu}{C_I} = \frac{C_C}{C_I} 2\sqrt{2}SWu \tag{6}$$

where the subscripts I and C refer to the instrument and the calibrator, respectively, and we have used (5). Almost every instrument produced by RSI has $C_C/C_I = 1$.

An alternative method of capturing the output of the shear probe is to connect it to a very high-impedance ($\approx$100 $\mathrm{G\Omega}$) voltage buffer. The charge produced in response to the bending of the beam produces a voltage because the probe has a capacitance of approximately 1 nF. The capacitance of the probes is temperature dependent. Thus, even if the charge produced per unit of mechanical excitation were independent of temperature, the voltage produced by a probe will still be temperature dependent. In addition, the lead capacitance must be accounted for in both the calibrator and in the instrument. The lead capacitance adds to the probe capacitance and reduces the output voltage. Most co-axial cables have a capacitance of 150 $\mathrm{nF\,m^{-1}}$. The output voltage from the shear probe calibrator using a *voltage* buffer is

$$\begin{aligned} E_C &= \sqrt{2}SU^2 \sin(2\alpha) \\ &= 2\sqrt{2}S(U\cos\alpha)(U\sin\alpha) \\ &= 2\sqrt{2}SWu \end{aligned} \tag{7}$$

which is identical to (4) but the value of the sensitivity, S, derived from a regression (3) may be different from that derived using a charge-transfer amplifier. The output from the voltage amplifier in the calibrator is determined by the capacitance of the probe itself acting in parallel with the capacitance of the cable connecting the probe to the voltage amplifier.

3 Shear-Probe Circuit

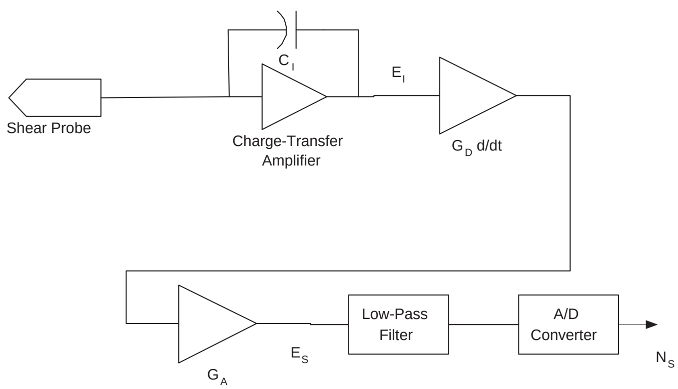

Figure 2: A block diagram of the shear probe circuit in a typical instrument.

The analog (continuous-domain) signal chain for the shear probe is depicted in Figure 2. The first stage is the charge-transfer amplifier that uses a capacitor, C_I, that produces the signal E_I described in (6). The second stage is the differentiator that produces the signal $G_D \mathrm{d}E_I/\mathrm{d}t$. This is followed by a frequency-independent gain G_A, that is almost always equal to 1, to produce the signal E_S given by

$$\begin{aligned} E_S &= \frac{C_C}{C_I} 2\sqrt{2} G_D G_A S W \; \frac{\mathrm{d}u}{\mathrm{d}t} \\ &= \frac{C_C}{C_I} 2\sqrt{2} G_D G_A S W^2 \; \frac{\mathrm{d}u}{\mathrm{d}z} \\ &= 2\sqrt{2} G_D S W^2 \; \frac{\mathrm{d}u}{\mathrm{d}z} \end{aligned} \tag{8}$$

where I have taken the usual case of $C_C = C_I$ and $G_A = 1$, and W is the speed of profiling in the direction z, with no particular geographic direction being implied by the symbol z. The next stage is an anti-aliasing low-pass filter. The last stage is a data sampler that converts the voltage E_S into a signed integer N_S given by

$$N_S = \frac{2^B}{V_{FS}} \; E_S = \frac{2^B}{V_{FS}} \; 2\sqrt{2} G_D S W^2 \; \frac{\mathrm{d}u}{\mathrm{d}z} \tag{9}$$

where B is the number of bits of the sampler (usually $B = 16$) and V_{FS} is the full-scale voltage range of the converter (usually $V_{FS} = 4.096\,\mathrm{V}$).

Conversion into physical units is simply a matter of using (9). The gain of the differentiator, G_D, is a characteristic of the circuit and is provided in the dynamic-calibration section of the report for your instrument (Figure 3). This parameter and the others (B and V_{FS}) that characterize your instrument must be the configuration-file of your instrument. These parameters are stable and do need need to be changed. The probe sensitivity, S, depends on the actual probe used, and is provided in a separate calibration report. It too must be in the configuration-file, and it must be updated whenever you change probes. A configuration-file containing the parameters for your instrument are shipped with your instrument. However, the sensitivity parameter, S, is only a nominal value.

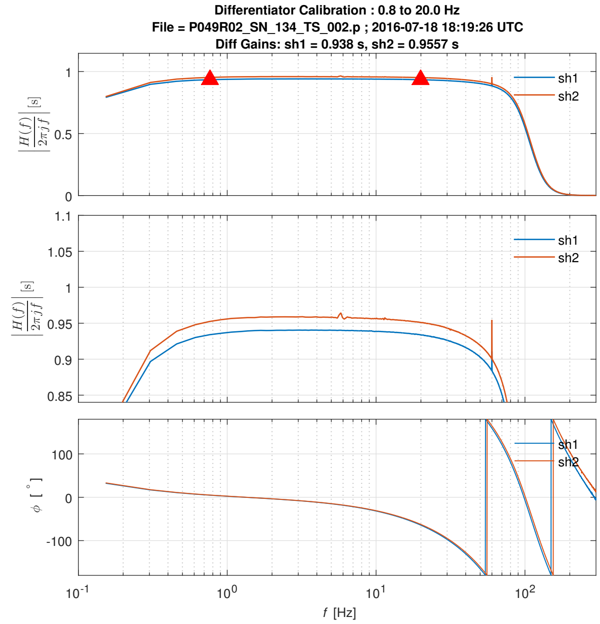

Figure 9: Transfer function of the shear probe circuits, relative to that of an ideal differentiator. The charge-transfer amplifier responds only to AC signals and has its half-power response at 0.1 Hz. The gains of the differentiators are indicated in the upper panel and represent the mean gain between the frequency limits indicated by the red triangles. Input signal was 2Vpp. Upper panel: Gain with respect to frequency. Middle panel: Same but with zoom-in view. Lower panel: phase with respect to frequency.

Figure 3: A typical dynamic calibration of the shear probe circuit to determine the gain of the differentiator.

3.1 Wavenumber Response of Shear Probes

The shear probe has a finite size and consequently smoothes fluctuations with spatial scales comparable to, and smaller than, the size of the probe. This spatial averaging has been examined by Macoun and Lueck [4] who recommend that the probes produced by RSI have their spectra corrected by the factor

$$\Phi(k) = 1 + \left(\frac{k}{50}\right)^2 \tag{10}$$

where k is the wavenumber in units cycles per meter [cpm] and 50 cpm is the half-power wavenumber response of the shear probe.

3.2 Water Density Effects

The bending force on the shear probe is proportional to the dynamic pressure over its surface, ρU^2. The shear probes are usually calibrated at room temperature ($20 - 25\,^\circ$C) in fresh water which has a density of $\rho = 997 - 998\,\mathrm{kg\,m^{-3}}$, and this density is 2 to 3 % smaller than the typical density of seawater. Users may scale up the sensitivity, S, according to the in *situ* density.

4 Thermistor Fundamentals

Thermistors are negative temperature-coefficient metal oxides. The blend of metal oxides determines the resistance of a thermistor and its temperature-coefficient of resistance. Metal oxides have a temperature-coefficient of resistance of about $\hat{\alpha} \approx -0.04\,°\mathrm{C}^{-1}$, which is many tens of times larger than the coefficient of metals, and this makes them suitable for detecting small fluctuations of temperature. They can also be manufactured to very small dimensions, which allows them to respond quickly to changes of temperature. The FP07 thermistor (Figure 4) has its sensing element (the black dot at the tip) mounted into a glass substrate (the bulbous feature behind the tip). The sensing tip of metal oxide has a diameter of 180 µm and is coated with glass to a thickness of approximately 50 µm. The response time of the FP07 in water is about 7 ms at speeds of $1\,\mathrm{m\,s^{-1}}$. The response time decreases with increasing speed. Neither the actual time response, nor its dependence on speed, have been convincingly determined by the scientific community. A range of values, and response forms have been reported. [**?**] provides the most recent discussion. The metal-oxide bead of the FP07 thermistor is hand-placed and hand-fused to the bulbous glass substrate. Therefore, the tip geometry varies among units and it is almost certain that the response characteristics will also vary. There are no facilities for routinely calibrating the frequency response of thermistors.

Figure 4: A photograph of the FP07 thermistor mounted into a sting by RSI.

The resistance of a thermistor follows approximately the Steinhart-Hart equation [5] which was developed for semiconductors, even though metal-oxide is not a true semiconductor. In its simplest form the Steinhart-Hart equation relates resistance to temperature using

$$\frac{R_T}{R_0} = \exp\left(\beta\left[\frac{1}{\hat{T}} - \frac{1}{\hat{T}_0}\right]\right) \tag{11}$$

where R_T is the resistance of the thermistor, $\hat{T}$ is the absolute temperature (in units of kelvin), R_0 is the resistance at the temperature $\hat{T}_0$, and β is a “material constant” that depends on the specific mixture of metal-oxides[1]. The FP07 thermistor provided by RSI has $R_0 \approx 3000\,\Omega$ at

[1]Absolute temperature (expressed in units of Kelvin) is represented by a symbol with a hat (ˆ), while temperature expressed in units of Celsius will be hatless. Therefore, $\hat{T} = 273.15 + T$

17 °C. It is difficult and costly for the manufacturer to precisely control R_0, and the typical uncertainty of this value is ±25 %. The material constant β is controlled fairly precisely and usually varies by only ∼1 % within a production batch and only a little more between batches. The range of the resistance ratio R_T/R_0 is approximately 0.5 to 2 for the range of temperature in the ocean.

The thermistor is usually calibrated using

$$\frac{1}{\hat{T}} = \frac{1}{\hat{T}_0} + \frac{1}{\beta_1}\log_e\left(\frac{R_T}{R_0}\right) + \frac{1}{\beta_2}\log_e^2\left(\frac{R_T}{R_0}\right) \quad . \tag{12}$$

The linear version of (12) is accurate to about ±0.05 °C over the oceanic temperature range, while the second-order form is accurate to 0.005 °C (see appendix A). There is no justification for using a higher order equation because the FP07 thermistor is unprotected from the pressure of water and will compress with increasing depth and, thereby reduce its resistance [6]. For comparison, Sea-Bird calibrates their SBE-3F thermometers, which are pressure protected, using a fourth-order version of (12).

5 Thermistor Circuit

5.1 Deriving the temperature using N_T or N_{T_dT}

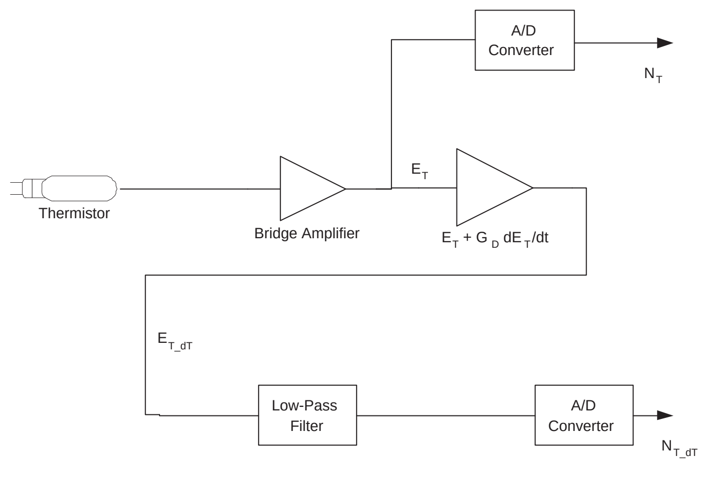

Figure 5: A block diagram of the thermistor circuit in a typical instrument.

A typical block diagram of the circuit supporting the FP07 thermistor is shown in Figure 5. The thermistor, R_T, is one arm of a four-arm Wheatstone bridge. The other three arms are resistors of value $R_0 = 3000\,\Omega$. The output, E_T of the bridge amplifier is

$$E_T = \frac{1}{2} G E_B \left(\frac{1 - R_T/R_0}{1 + R_T/R_0} \right) \tag{13}$$

where G is the gain of the bridge amplifier (typically 6 $\pm 0.1\,\%$), and E_B is the bridge excitation voltage (typically 0.682 V). The precise values are given in the calibration report for your instrument[2] and these values are quite stable. The signal E_T is also passed through a pre-emphasizer to produce the signal

$$E_{T\_dT} = E_T + G_D\ \mathrm{d}E_T/\mathrm{d}t \tag{14}$$

where G_D is the gain of the time-derivative amplifier in the circuit. Typically, $G_D \approx 1$ s (Figure 6).

Both the basic temperature signal, E_T and the pre-emphasized signal, E_{T_dT}, are sent to a data sampler (analog-to-digital converter) to produce the signed integers,

$$N_T = \frac{2^B}{V_{FS}} E_T \tag{15}$$

and

$$N_{T\_dT} = \frac{2^B}{V_{FS}} E_{T\_DT} \tag{16}$$

where B is the number of bits of the sampler (usually $B = 16$) and V_{FS} is the full-scale range of the sampler (usually $V_{FS} = 4.096$ V).

[2]Not the report for your thermistor.

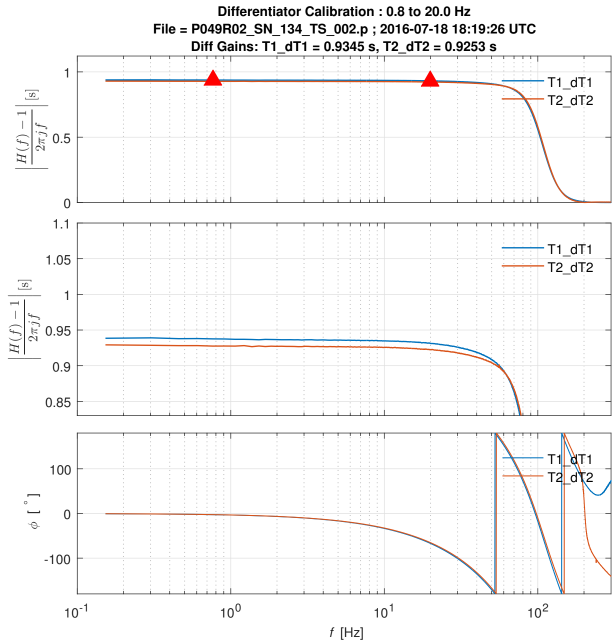

Figure 10: Transfer function of the pre-emphasized thermistor circuits, relative to that of an ideal differentiator. The gains of the differentiators are indicated in the upper panel and represent the mean gain between the frequency limits indicated by the red triangles. Input signal was 2Vpp. Upper panel: Gain with respect to frequency. Middle panel: Same but with zoom-in view. Lower panel: phase with respect to frequency.

Figure 6: A typical dynamic calibration of the thermistor circuit to determine the gain of the differentiator, G_D.

Analog electrical circuits are never perfect, so the entire amplification and sampling chain is calibrate using precision (0.01 %) resistors in place of the thermistor, R_T. The output signals, N_T and N_{T_dT}, are regressed against the expected outputs using

$$N_T = a_0 + b_0 \left[\frac{2^B}{V_{FS}} \frac{1}{2} G E_B \left(\frac{1 - R_T/R_0}{1 + R_T/R_0} \right) \right] = a_0 + b_0 x \tag{17}$$

and

$$N_{T\_dT} = a_1 + b_1 \left[\frac{2^B}{V_{FS}} \frac{1}{2} G E_B \left(\frac{1 - R_T/R_0}{1 + R_T/R_0} \right) \right] = a_1 + b_1 x \tag{18}$$

where x is the term in square braces and equals the right-hand side of (15). x should also represent the right-hand side of (16) because $\mathrm{d}E_T/\mathrm{d}t = 0$ for a static calibration. The linear regression coefficients a_i and b_i may be slightly different for the signal with pre-emphasis compared to the one without pre-emphasis because they are independent analog channels. Ideally, $a_i = 0$ and $b_i = 1$ and, typically, $|a_i| \leq 15$ and b is within 0.1 % of unity. The resultant fit of $a_0 + b_0 x$ to N_T is usually within ± 0.5 counts (Figure 7). However, the fit of $a_1 + b_1 x$ to N_{T_dT} is slightly poorer because the pre-emphasis adds noise to this signal, and this makes the coefficients a_1 and b_1 less reliable than their counterparts in (17).

To derive the actual thermistor resistance ratio, R_T/R_0, we use the inverse of (17), namely

$$\frac{R_T}{R_0} = \frac{1 - Z}{1 + Z} \tag{19}$$

where

$$Z = \frac{N_T - a_0}{b_0} \frac{V_{FS}}{2^B} \frac{2}{GE_B} \quad . \tag{20}$$

The computed resistance ratio can then be converted into physical units using (12).

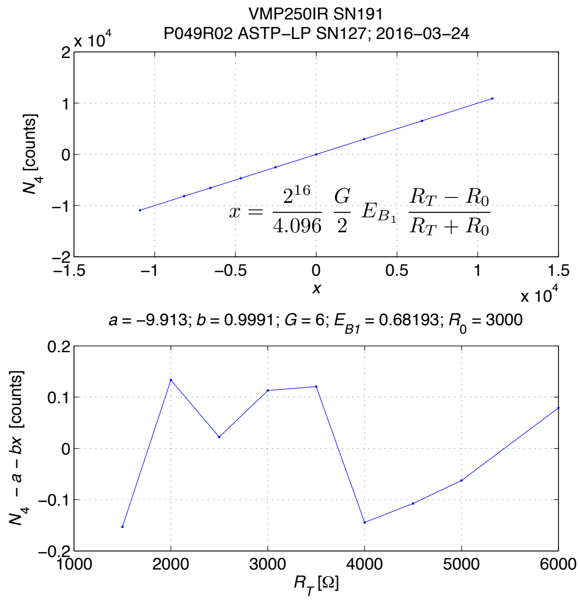

Figure 7: A typical static calibration of the electronics supporting an FP07 thermistor. N_4 is identical to N_T discussed here.

The pre-emphasized signal, N_{T_dT}, contains both the temperature and its time-derivative. It is converted into a "temperature" signal by low-pass filtering it using a first-order filter with a cut-off frequency of $(2\pi G_D)^{-1}$. This filter removes the derivative portion of the signal and produces a new signal, N_{T_hres}, that has a resolution which about 100 times finer than the signal N_T. This is explained in Technical Note 002 and in [7].

The signals N_{T_hres} and N_T are nominally identical, except for statical fluctuations due to the higher noise level of N_T. However, they are also systematically different because they are derived from independent signal paths, which is the reason that the pairs $[a_0\ a_1]$ and $[b_0\ b_1]$ are not identical in (17 and 18). Because the values of a_0 and b_0 are more reliable than their counterparts for the pre-emphasized signal, we regress N_{T_hres} against N_T (to first order) so that we can use the coefficients a_0 and b_0 to convert this high-resolution signal into temperature in physical units, T_{hres}, using (19 and 12).

Because the relationship between temperature, T, and the data samples, N_T, is rather complicated, it is frequently held that this relationship is highly non-linear. It is actually fairly close to linear. For example, a first-order regression of temperature against N_T is accurate to $\sim \pm 1\,\mathrm{K}$ over the oceanic range of temperature. The computational burden of deriving temperature using (12) is not significant, if one is careful to call the log-function only once.

5.2 Deriving the gradient of temperature

There are two methods for deriving the gradient of temperature in the direction of profiling. The first method is achieved by taking the first difference of the high-resolution temperature T_{hres}. The second method is achieved by means of high-pass filtering the signal N_{T_dT} and then converting that into physical units. Both procedures produce the time rate-of-change of temperature, $\mathrm{d}T/\mathrm{d}t$. Dividing this by the speed of profiling produces the gradient of temperature in the direction of profiling, for example $\partial T/\partial z = W^{-1}\mathrm{d}T/\mathrm{d}t$ for the case of a vertical profiler, where W is the magnitude of the vertical velocity of the profiler.

5.2.1 Temperature gradient by way of first-difference

The high-resolution temperature signal T_{hres} has extremely low noise and this makes it possible to estimate the time rate-of-change of temperature using a first-difference operation. Specifically,

$$\frac{\mathrm{d}T}{\mathrm{d}t} = \frac{T_{hres}(n) - T_{hres}(n-1)}{\Delta t} = f_s \left(T_{hres}(n) - T_{hres}(n-1)\right) \tag{21}$$

where f_s is the sampling rate and n is the index to the samples. However, this is only an *approximation* of a time derivative because a derivative is a continuous-domain concept, whereas the data, T_{hres}, are samples and reside in the discrete domain. The z-transform [7] of the right-hand side of (21) is

$$\begin{aligned} H(z) &= f_s \left(1 - z^{-1}\right) = f_s \; z^{-1/2} \left(z^{1/2} - z^{-1/2}\right) \\ &= 2f_N \; \exp\left(-j\frac{\pi}{2}\frac{f}{f_N}\right)\left[\exp\left(j\frac{\pi}{2}\frac{f}{f_N}\right) - \exp\left(-j\frac{\pi}{2}\frac{f}{f_N}\right)\right] \\ &= 4f_N \; \exp\left(j\frac{\pi}{2}\left[1 - \frac{f}{f_N}\right]\right)\sin\left(\frac{\pi}{2}\frac{f}{f_N}\right) \end{aligned} \tag{22}$$

where $f_N = f_s/2$ is the Nyquist frequency and the z-transform is evaluated on the unit circle $z = \exp(j\pi f/f_N)$. For frequencies small compared to f_N, the transfer function (22) reduces to $2\pi jf$ which is identical to the transfer function of a continuous-domain time derivative. However, at the Nyquist frequency, where $z = -1$, the discrete-domain approximation has a transfer function of $4f_N$ rather than $2\pi jf_N$ – it is too small by a factor $\pi/2$ – and its phase is zero instead of $\pi/2$. Spectra of the temperature gradient must be boosted by a factor of $(2\pi f/|H|)^2$ to correct for the estimation by way of first difference.

An additional, and more subtle, correction must be made to account for the difference between a continuous-domain low-pass filter and its approximation in the discrete domain. The pre-emphasis was applied in the continuous domain, but it is removed in the discrete domain. It is quite common to convert continuous-domain filters into discrete-domain equivalent filters using the bi-linear transformation [7]. This is the default mapping used by Matlab. The bi-linear transformation maps the imaginary axis of the complex plain of the Laplace transform on to the unit circle of the complex plain of the z-transform. Zero frequency of both domains are identical. However, infinite frequency of the continuous domain is mapped to the Nyquist frequency of the discrete domain. The transfer functions of the filters in the two domains are nearly identical for $f \lesssim f_N/3$ but the transfer functions diverge sharply for higher frequency where a discrete-domain low-pass filter attenuates a signal more strongly than its continuous domain equivalent filter. This is often call "frequency warping". The relative response of the two filters can be evaluated using the Matlab function `freqz`, and a correction is applied to temperature gradient spectra by functions in the ODAS Matlab Library for frequencies up to $0.9f_N$.

In summary;

- Use the procedures of section 5.1 to derive the absolute temperature $\hat{T}$, in units of kelvin, or its equivalent in units of °C.
- Apply the first-difference operation of (21) to approximate $\mathrm{d}T/\mathrm{d}t$.
- Divide this signal by the speed of profiling to get the gradient of temperature, $\mathrm{d}T/\mathrm{d}z$, in the direction of profiling, z. No particular direction is implied by the usage of z.

Spectra of temperature gradient must be corrected for the frequency dependence of a first-difference operator (22), and for the low-pass filter used to derive the temperature $\hat{T}$ (see discussion above).

5.2.2 Temperature gradient by way of high-pass filter

The pre-emphasized signal, N_{T_dT}, contains both the temperature signal and its time derivative (14 and 16) and, so, the derivative can be obtained by removing the temperature portion of this signal. The continuous-domain transfer function of the pre-emphasis is

$$H_{T\_dT}(f) = 1 + 2\pi j G_D f \quad . \tag{23}$$

Therefore, applying a first-order, high-pass filter with a cut-off frequency of $(2\pi G_D)^{-1}$, namely

$$H_{HP}(f) = \frac{2\pi j G_D f}{1 + 2\pi j G_D f} \tag{24}$$

removes the temperature portion of the signal, N_{T_dT}, and leaves only the derivative multiplied by G_D. That is, if we multiply (23) by (24), the result is $2\pi j G_D f$ which is the frequency domain representation of a time derivative operation multiplied by the factor G_D. The filtering must be done in the discrete domain. However, in this case, frequency warping is negligible because (i) the cut-off frequency is very much smaller than the Nyquist frequency, $f_N \ggg (2\pi G_D)^{-1}$ and (ii) the response (24) asymptotes to unity, making it independent of frequency, for $f \gg (2\pi G_D)^{-1}$.

Let N_{dT} denote the signal N_{T_dT} after it is high-pass filtered and divided by G_D. How can it be converted into physical units? Using (13, 14, 16, and 18) we have

$$\begin{aligned} N_{dT} &= \frac{b}{2}\,\frac{2^B}{V_{FS}} G\; E_B\;\frac{\mathrm{d}}{\mathrm{d}t}\left(\frac{1 - R_T/R_0}{1 + R_T/R_0}\right) \\ &= \eta \frac{\mathrm{d}}{\mathrm{d}t}\left(\frac{1 - R_T/R_0}{1 + R_T/R_0}\right) \\ &= -\eta\;\frac{1}{1 + R_T/R0}\;\frac{\mathrm{d}}{\mathrm{d}t}\left(\frac{R_T}{R_0}\right) - \eta\frac{1 - R_T/R_0}{(1 + R_T/R_0)^2}\frac{\mathrm{d}}{\mathrm{d}t}\left(\frac{R_T}{R_0}\right) \\ &= -\frac{2\eta}{(R_T/R_0 + 1)^2}\;\frac{\mathrm{d}}{\mathrm{d}t}\left(\frac{R_T}{R_0}\right) \end{aligned} \tag{25}$$

where the scale coefficients have been lumped into η for simplicity, that is

$$\eta = \frac{b}{2} \frac{2^B}{V_{FS}} G \; E_B \quad . \tag{26}$$

The Steinhart-Hart equation (12) allows us to express the rate-of-change of temperature to the rate-of-change of the thermistor resistance, namely

$$-\frac{1}{\hat{T}^2} \frac{\mathrm{d}T}{\mathrm{d}t} = \left(\beta_1 \frac{R_T}{R_0}\right)^{-1} \left[1 + 2\frac{\beta_1}{\beta_2} \log\left(\frac{R_T}{R_0}\right)\right] \frac{\mathrm{d}}{\mathrm{d}t} \left(\frac{R_T}{R_0}\right) \tag{27}$$

where T can be the temperature in °C or K. The second term in the square braces is small because $\beta_1/\beta_2 \sim 0.01$ and the logarithm of the resistance ratio is in the range of ± 1. Using (25) we have

$$\frac{\mathrm{d}T}{\mathrm{d}t} = \frac{1}{2} \frac{\hat{T}^2}{\eta \beta_1} \frac{(R_T/R_0 + 1)^2}{R_T/R_0} \left[1 + 2\frac{\beta_1}{\beta_2} \log\left(\frac{R_T}{R_0}\right)\right] N_{dT} \quad . \tag{28}$$

The product of all of the variables that multiply N_{dT} on the right-hand side of (28) is nearly constant. The contents of the square braces is very close to 1. The factor involving the resistance ratio varies from 4 to 4.5. The square of the absolute temperature varies by one-eighth around 290^2. Thus, using typical values

$$\frac{\mathrm{d}T}{\mathrm{d}t} \approx 1.7 \times 10^{-3} \; N_{dT} \quad . \tag{29}$$

In summary;

- Use the procedures of section 5.1 to derive the absolute temperature $\hat{T}$.
- High-pass filter the raw pre-emphasized signal, N_{T_dT}, using a first-order filter with a cut-off frequency of $(2\pi G_D)^{-1}$, in units of Hz.
- Divide this signal by G_D to produce the signal N_{dT}.
- Gather the thermistor coefficients, $\hat{T}_0$, β_1, and β_2 that were derived from its calibration. If you do not have β_2 set it to infinity.
- Gather the circuit coefficients that comprise η, (26).
- Apply (28) to compute the rate-of-change of temperature, $\mathrm{d}T/\mathrm{d}t$.
- Divide this signal by the speed of profiling to get the gradient of temperature, $\mathrm{d}T/\mathrm{d}z$, in the direction of profiling, z. No particular direction is implied by the usage of z.

Finally and most importantly, no correction needs to be applied when using this high-pass filter method to determine the gradient of temperature.

5.3 Comparing first-difference and high-pass methods

A profile taken off the coast of Chile in 2012, with a VMP-250, has significant temperature gradient microstructure (Figure 8) which makes it suitable for comparing the two methods of calculating the gradient of temperature. The time series for the pressure (depth) range of 92 to 163 dbar (Figure 9) has gradients exceeding $2\,\mathrm{K\,m^{-1}}$. However, the difference between the two methods is small and the trace derived using the method of first-difference completely covers the trace derived using the high-pass method. The data were sampled at a rate of $512\,\mathrm{s^{-1}}$.

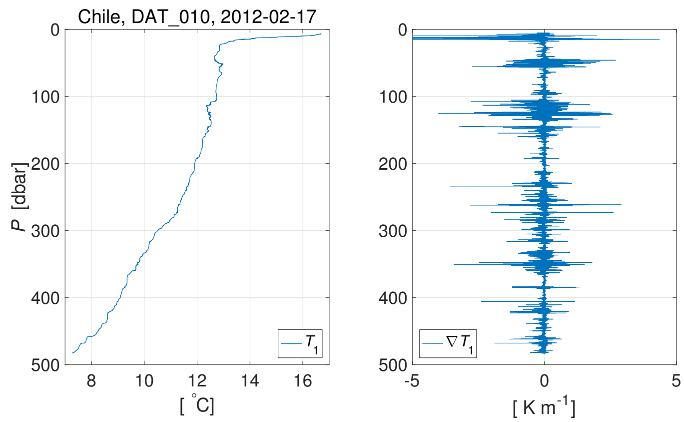

Figure 8: A profile of temperature (left) and its gradient (right) taken off the coast of Chile with a VMP-250 vertical profiler.

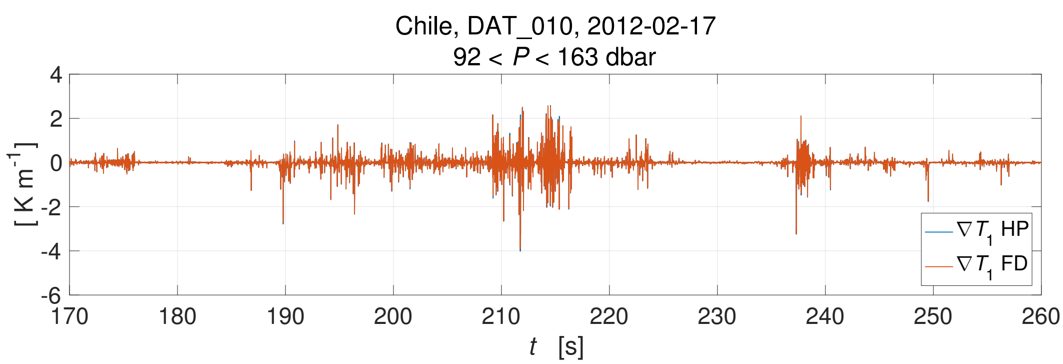

Figure 9: The time series of temperature gradient for the depth range of 92 to 163 dbar. The labels HP and FD identify the methods of high-pass and first-difference, respectively.

The difference between the two methods is apparent in the spectra of the two signals (Figure 10). The spectra are nearly indistinguishable for frequency up to ∼50 Hz, above which the spectrum derived by the first difference method (red line) systematically falls below the spectrum derived by the high-pass method. Beyond 150 Hz (∼60 % of the Nyquist frequency) the spectrum for the signal derived by the first-difference technique decreases rapidly towards zero with increasing frequency, due to frequency warping. However, the spectrum of the signal derived by the high-pass method levels off to the sampling noise of the original pre-emphasized signal. In this case, about $5\times10^{-9}\,\mathrm{K^2\,m^{-2}\,Hz^{-1}}$. More than 90 % of the variance of the two signals resides at frequencies lower than 50 Hz and, consequently, there is little visual difference between the time traces of the two signals.

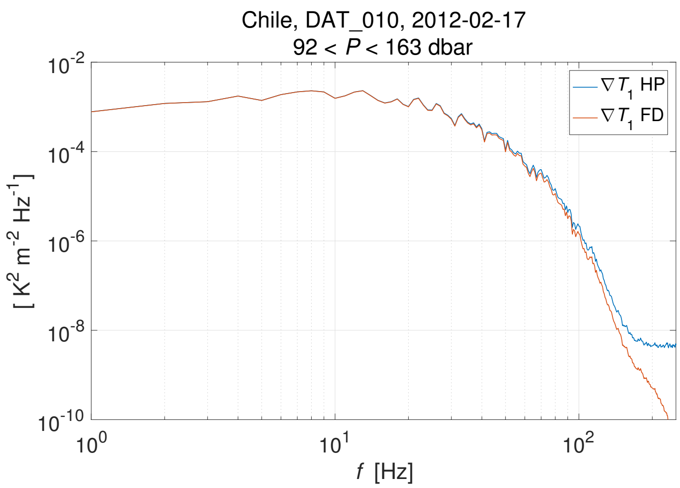

Figure 10: The spectra of the temperature gradient derived using the high-pass (blue) and first-difference (red) methods.

A more quantitative way of comparing the two methods is to plot the ratio of the two spectra (Figure 11). They differ by 10 % at 55 Hz and by a factor of 2 at 127 Hz.

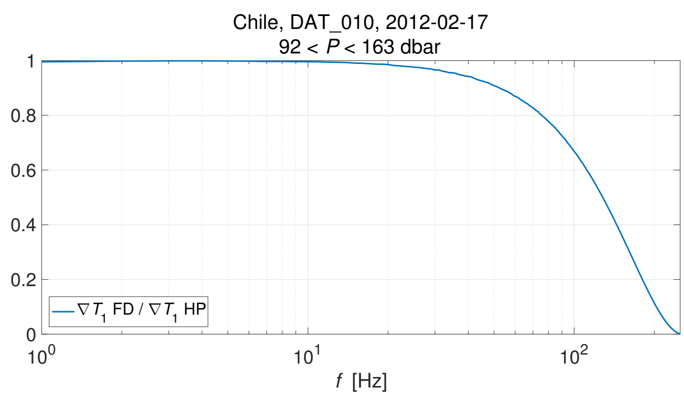

Figure 11: The ratio of the temperature gradient spectrum derived using the first-difference method to the spectrum derived using the high-pass method.

6 Micro-conductivity Fundamentals

A conductivity sensor and its electronics can measure only the *conductance* of the fluid surrounding its electrodes. It cannot measure the *conductivity* of the fluid directly. This is a material-specific property. The micro-conductivity sensor used by RSI is manufactured by Sea-Bird Inc. to the specifications of RSI (Figure 12). Its two electrodes are on the ends of "needles', and have the shape of a disk with a diameter of $\sim$1 mm. The centres of the electrodes are separated by $\sim$1.5 mm. The electronics applies an AC-voltage across the electrodes and measures the resultant current. The ratio of current-to-voltage is a measure of the conductance of the portion of the fluid that provides an electrical path between the electrodes. This conductance is proportional to the fluid conductivity, but its value depends also on the geometry, orientation, separation and dimensions of the electrodes. It is usual to assign all these factors to a single "cell-constant", K, so that the measured conductance is

$$Y = KC \tag{30}$$

where Y is the conductance (in units of siemens), C is the fluid conductivity (in units of siemens/m), and K is the cell constant (in units of m). Only for very simple geometries is it possible to derive the cell constant analytically because the current path between the electrodes is usually very complicated. It is often falsely assume that the cell constant is actually constant for a given sensor. However, this is never completely true. Aside from the obvious change of the cell constant resulting from bending the needles that hold the electrodes (Figure 12), the cell constant may change due to thermal expansion and pressure induced contraction.

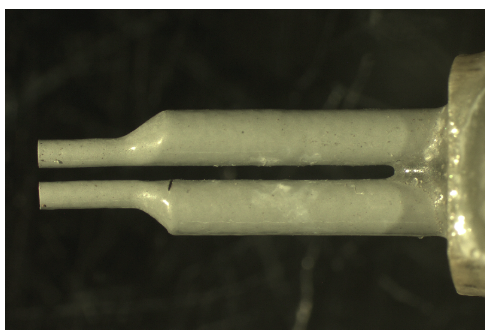

Figure 12: A photograph of the SBE7 micro-conductivity sensor mounted into a sting for RSI.

The surface of the electrodes of the sensor supplied by RSI is coated with platinum black, which is a soft and sponge-like coating that increases the surface area in contact with the fluid. Mechanical abrasion of the platinum-black coating will change the conductance measured by the sensor. Similarly, the measured conductance will change if material adheres to the electrode surface, such as silt or gelatinous biological films. The sensor must, therefore, be cleaned after use and, if possible, pre-wetted. If you have some knowledge of the expected conductivity (say, from a CTD) and if the conductivity reported by the micro-conductivity sensor differs significantly from the known (or expected) value, then the data might be salvaged by adjusting the value of the cell constant that is used to convert your data into physical units (which is discussed next).

7 Micro-conductivity Circuit

The micro-conductivity board applies a sinusoidal voltage difference between the electrodes of a conductivity cell. The waveform has a very stable amplitude of approximately 0.2 V and a frequency of $f_0 = 7812.50$ Hz. The current through the electrodes is converted into a voltage and synchronously rectified[3]. The resultant signal consists of a mean that is proportional to the amplitude of the electrode current plus the fundamental frequency, f_0, and its harmonics. It looks like a periodic repetition of $\sin\theta$ for $0 < \theta \leq \pi$. This signal is then sharply low-pass filtered at 1000 Hz to remove all harmonics and leave only the amplitude portion of the signal. This filtered signal then splits into two paths. In the first path, it is pre-emphasized by adding a fraction of its time-rate-of change, after which it is anti-alias filtered (usually at 100 Hz) to produce the signal E_{C_dC}. It is then sampled to produce N_{C_dC}. The second path, does not have pre-emphasis and goes directly to an anti-alias filter to create the signal E_C which is sampled to produce N_C. Some boards do not have this second path.

7.1 Deriving the conductivity using N_{C_dC} and N_C

The electronics board supporting the micro-conductivity sensor is quite linear with respect to conductance (Figure 13). The static response of the board is calibrated by substituting precision (0.01 %) resistors in place of a real sensor. Readings of the measured output are then regressed against the applied conductance to derive the offset- and slope-coefficients of a and b, respectively. The units of a and b are V and V S^{-1}, respectively.

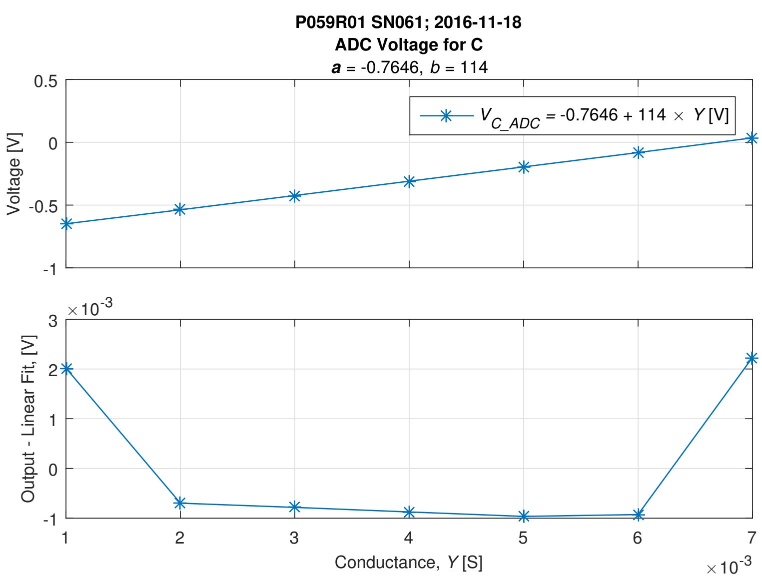

Figure 13: The static calibration of a micro-conductivity circuit. Upper trace; the circuit output voltage with respect to applied conductance. Lower panel; the deviation of the least-squares fit, based on the coefficients shown in the title.

[3]Synchronous rectification is mathematically described by taking a sine wave and multiplying it by a square wave with an amplitude of 1 and a frequency and phase identical to that of the sine wave, namely $\operatorname{sign}(\sin(2\pi f_0 t))\,\sin(2\pi f_0 t)$.

The board calibration coefficients are used to convert the raw data into physical units of conductance, and these coefficients are time and temperature stable. The coefficients must be entered into your configuration-file, and this is usually done at RSI before shipping your instrument. The cell constant, K, of a micro-conductivity sensor is determined separately by immersing the sensor in a fluid of known conductivity. This constant is probe specific and must also be entered into the configuration-file for your instrument, and it must be updated whenever you change the sensor.

The output voltage of the circuit is pre-emphasized by adding a scaled time-derivative of the signal itself. It is then anti-alias filtered and sampled to produce the raw data

$$N_{C\_dC} = \frac{2^B}{V_{FS}} E_{C\_dC} = \frac{2^B}{V_{FS}} \left(E_C + G_D \frac{\mathrm{d}E_C}{\mathrm{d}t} \right) \tag{31}$$

where B is the number of bits in the sampler, V_{FS} is the full-scale voltage range of the sampler, and G_D is the gain of the differentiator used to pre-emphasize the voltage signal E_C, given by

$$E_C = a + bY \tag{32}$$

and Y is now the conductance of the fluid.

The pre-emphasized and sampled signal N_{C_dC} contains both the conductance signal and its rate-of-change. It is converted into a high-resolution conductance signal, $N_{C_{hres}}$, by passing it through a first-order low-pass Butterworth filter with a cut-off frequency of $(2\pi G_D)^{-1}$. This is explained in Technical Note 002 and in [7]. On some instruments the signal E_C is also sampled to produce the data N_C, but it will be a much lower resolution version of the one derived by low-pass filtering. Its main purpose is to confirm the accuracy of the low-pass filter operation.

Converting $N_{C_{hres}}$ into physical units is a matter of using (30—32) to derive the conductance of the fluid between the electrodes

$$Y = \frac{1}{b} \left(\frac{V_{FS}}{2^B} \, N_{C_{hres}} - a \right) \tag{33}$$

from which the fluid conductivity is obtained using

$$C_{hres} = \frac{Y}{K} = \frac{1}{b} \left(\frac{V_{FS}}{2^B} \, N_{C_{hres}} - a \right) \frac{1}{K} \quad . \tag{34}$$

This conductivity is in units of $\mathrm{S\,m^{-1}}$ and is converted to units of $\mathrm{mS\,cm^{-1}}$ by multiplying it by a factor of 10. If your instrument does provide the data N_C (which are the samples of E_C), then you can use (34) to convert these data into physical units. The values of a and b might differ slightly from the ones used for the high-resolution conductivity.

7.2 Deriving the gradient of conductivity

There are two methods for deriving the gradient of conductivity in the direction of profiling. The first method is achieved by taking the first difference of the high-resolution conductivity C_{hres}. The second method is achieved by means of high-pass filtering the signal N_{C_dC} and then converting that into physical units. Both methods produce the time rate-of-change of conductivity, $\mathrm{d}C/\mathrm{d}t$. Dividing this by the speed of profiling produces the gradient of conductivity in the direction of profiling, for example $\partial C/\partial z = W^{-1}\mathrm{d}C/\mathrm{d}t$ for the case of a vertical profiler, where W is the magnitude of the vertical velocity of the profiler.

7.2.1 Conductivity gradient by way of first-difference

The high-resolution conductivity signal C_{hres} has extremely low noise and this makes it possible to estimate the time rate-of-change of conductivity using a first-difference operation. Specifically,

$$\frac{\mathrm{d}C}{\mathrm{d}t} = \frac{C_{hres}(n) - C_{hres}(n-1)}{\Delta t} = f_s \left(C_{hres}(n) - C_{hres}(n-1) \right) \tag{35}$$

where f_s is the sampling rate and n is the index to the samples. However, this is only an *approximation* of a time derivative because a derivative is a continuous-domain concept, whereas the data, C_{hres}, are samples and reside in the discrete domain. The implications of a first-difference operation are discussed in section 5.2.1 and will not be repeated here.

7.2.2 Conductivity gradient by way of high-pass filter

The pre-emphasized signal, N_{C_dC}, contains both the conductivity signal, E_C, and its time derivative (32 and 31). The derivative portion is obtained by removing the conductivity portion. The continuous-domain transfer function of the pre-emphasis is

$$H_{C\_dC}(f) = 1 + 2\pi j G_D f \quad . \tag{36}$$

Therefore, applying a first-order, high-pass filter with a cut-off frequency of $(2\pi G_D)^{-1}$, namely

$$H_{HP}(f) = \frac{2\pi j G_D f}{1 + 2\pi j G_D f} \tag{37}$$

removes the conductivity portion of the signal, E_C, leaving only the derivative multiplied by G_D. That is, if we multiply (36) by (37), the result is $2\pi j G_D f$ which is the frequency-domain representation of a time derivative operation multiplied by the factor G_D.

Let N_{dC} denote the signal N_{C_dC} after it is high-pass filtered and divided by G_D. Using (30, 31, and 32), this signal is

$$N_{dC} = \frac{2^B}{V_{FS}} \frac{\mathrm{d}E_C}{\mathrm{d}t} = \frac{2^B}{V_{FS}} b \frac{\mathrm{d}Y}{\mathrm{d}t} = \frac{2^B}{V_{FS}} bK \frac{\mathrm{d}C}{\mathrm{d}t} \quad . \tag{38}$$

Therefore, the rate-of-change of fluid conductivity is derived using

$$\frac{\mathrm{d}C}{\mathrm{d}t} = \frac{V_{FS}}{2^B} \frac{1}{bK} N_{dC} \tag{39}$$

where, to summarize, B is the number of bits of the sampler, V_{FS} is the full-scale voltage range of the sampler, b is the calibrated slope coefficient of the electronics, and K is the cell-constant of the conductivity sensor. Dividing the rate-of-change of conductivity by the speed of profiling gives the gradient of conductivity in the direction of profiling.

A A typical FP07 calibration report

ROCKLAND SCIENTIFIC

Rockland Scientific International Inc.
520 Dupplin Road, Victoria, BC. V8Z 1C1
Phone: (250) 370-1688 Fax: (250) 370-0234

FP–07 Temperature Probe Calibration Report

Probe SN:	T944
Date:	2014-08-28
Room Temp:	22.5 °C
Operator:	Shiro Yasuda
SBT1:	SN031509
SBT2:	SN031568
Probe Channel:	4

Linear Model:

$$\frac{1}{\hat{T}} = \frac{1}{\hat{T}_0} + \frac{1}{\beta}\log_e\left(\frac{R_T}{R_0}\right)$$

$$\beta = 2998.36\,\mathrm{K}$$
$$T_0 = 280.260\,\mathrm{K}$$

Second-order Model:

$$\frac{1}{\hat{T}} = \frac{1}{\hat{T}_0} + \frac{1}{\beta_1}\log_e\left(\frac{R_T}{R_0}\right) + \frac{1}{\beta_2}\left(\log_e\left(\frac{R_T}{R_0}\right)\right)^2$$

$$\beta_2 = 256\,353.27\,\mathrm{K}$$
$$\beta_1 = 2976.47\,\mathrm{K}$$
$$T_0 = 280.265\,\mathrm{K}$$

$$[\hat{T}] \equiv \mathrm{K}, \qquad T \equiv \hat{T} - 273.15\ [^\circ\mathrm{C}]$$

SBT1 SN031509 (°C)	SBT2 SN031568 (°C)	Probe T944 (counts)
1.327	1.326	-3651.9
1.348	1.348	-3637.6
5.459	5.457	-1045.5
5.481	5.480	-1031.4
5.514	5.512	-1011.2
10.411	10.409	2002.4
10.424	10.423	2010.1
10.448	10.447	2025.1
15.378	15.376	4932.5
15.388	15.386	4938.9
15.416	15.415	4955.3
20.400	20.398	7733.2
20.412	20.410	7740.4
20.441	20.440	7756.7
25.578	25.576	10417.2
25.585	25.584	10421.9
25.606	25.604	10431.1
30.219	30.218	12634.9
30.226	30.224	12636.1
30.245	30.244	12646.4

Figure 14: FP07 thermistor calibration report – page 1

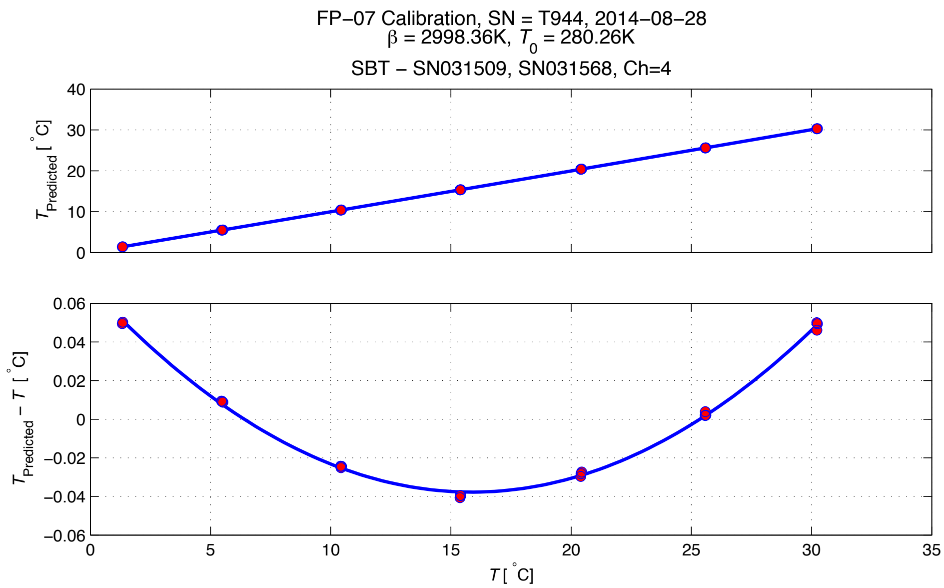

Figure 1: Linear Steinhart-Stein model. Upper panel; Predicted temperature versus measured temperature. Lower panel; Difference between the predicted and the measured temperature versus measured temperature.

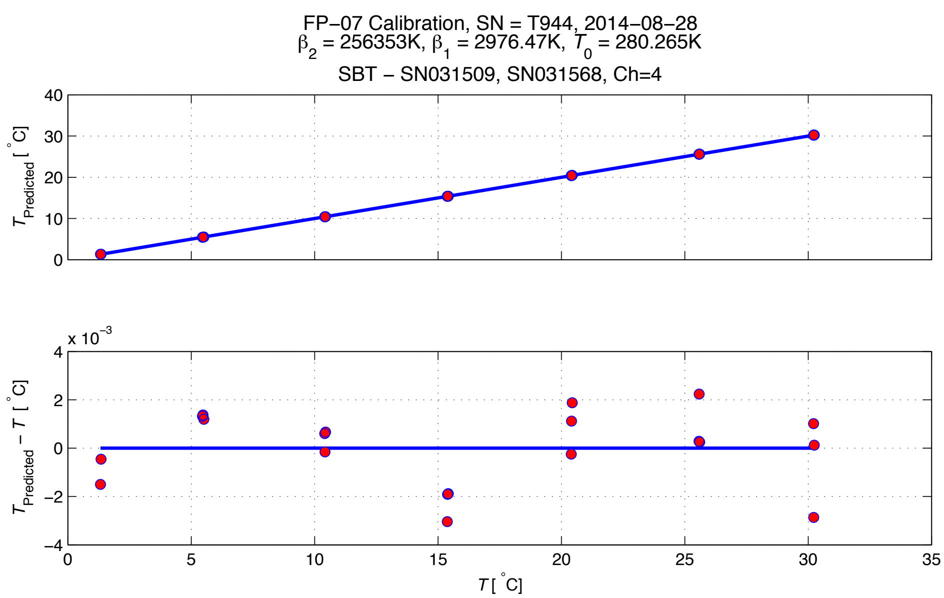

Figure 2: Second-order Steinhart-Stein model. Upper panel; Predicted temperature versus measured temperature. Lower panel; Difference between the predicted and the measured temperature versus measured temperature.

2

Figure 15: FP07 thermistor calibration report – page 2

B A typical micro-conductivity calibration report

Rockland Scientific International Inc.
520 Dupplin Road, Victoria, BC. V8Z 1C1
Phone: (250) 370-1688 Fax: (250) 370-0234

SBE7 MicroConductivity Probe Calibration Report

Probe SN:	C215
Date:	2016-07-08
Room Temp:	22.1 °C
Operator:	Shiro Yasuda
SBC1:	SN3136
SBC2:	SN1012
μC-LP P059R00:	SN001
Probe Channel:	2

SBC1 SN3136 (mS cm^{-1})	SBC2 SN1012 (mS cm^{-1})	Probe C215 (counts)
0.000	0.000	-7553.2
0.053	0.052	-7543.1
20.705	20.697	-3170.6
31.795	31.790	-892.2
37.604	37.598	285.0

Cell Constant:

$$K = 0.001\,12\,\mathrm{m}$$
$$K' = 0.001\,12\,\mathrm{m}$$

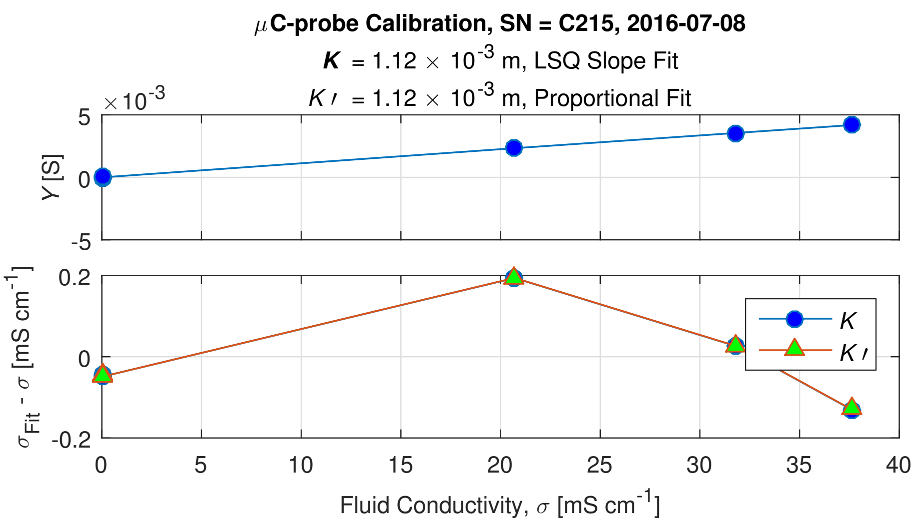

Figure 1: Upper panel; Probe conductance versus fluid conductivity. Lower panel; Difference between fitted and actual contuctivity using LSQ slope fit (blue) and proportional fit (green) versus fluid conductivity.

Figure 16: A micro-conductivity sensor calibration report.

References

[1] T. E. Siddon and H. S. Ribner. An aerofoil probe for measuring the transverse component of turbulence. *J. American Inst. Aeronautics and Astronautics*, 3:747–749, 1965.

[2] T. R. Osborn. Local vertical profiling of velocity microstructure. *Journal of Physical Oceanography*, 4:109–115, 1974.

[3] T. R. Osborn and W. R. Crawford. An airfoil probe for measuring turbulent velocity fluctuations in water. In F. W. Dobson and R. Davis, editors, *Air-Sea Interaction: Instruments and Methods*, Mechanical Engineering, page 535. Plenum, 1980.

[4] P. Macoun and R. Lueck. Modelling the spatial response of the airfoil shear probe using different sized probes. *Journal of Atmospheric and Oceanic Technology*, 21:284–297, 2004.

[5] John S. Steinhart and Stanley Hart. Calibration curves for thermistors. *Deep-Sea Research*, 15(4):497–503, 1968.

[6] Xiaodong Shang, Yongfeng Qi, Guiying Chen, Changrong Liang, Rolf G. Lueck, Brett Prairie, and Hua Li. An expendable microstructure profiler for deep ocean measurements. *Journal of Atmospheric and Oceanic Technology*, 34:1 – 15, 2017.

[7] T. D. Mudge and R. G. Lueck. Digital signal processing to enhance oceanographic observations. *Journal of Atmospheric and Oceanic Technology*, 11:825–836, 1994.

End of Document